Copper Complexes Hot Paper

How to cite: *Angew. Chem. Int. Ed.* **2021**, *60*, 23451 – 23462
International Edition: doi.org/10.1002/anie.202109367
German Edition: doi.org/10.1002/ange.202109367

A Copper(I) Complex with Two Unpaired Electrons, Synthesised by Oxidation of a Copper(II) Complex with Two Redox-Active Ligands

*Marco Werr, Elisabeth Kaifer, Markus Enders, Andika Asyuda, Michael Zharnikov, and Hans-Jörg Himmel**

Abstract: *Two homoleptic copper(II) complexes $[Cu(L1)_2]$ and $[Cu(L2)_2]$ with anionic redox-active ligands were synthesised, one with urea azine (L1) and the other with thio-urea azine (L2) ligands. One-electron oxidation of the complexes initiates an unprecedented redox-induced electron transfer process, leading to monocationic copper(I) complexes $[Cu(L1)_2]^+$ and $[Cu(L2)_2]^+$ with two oxidised ligands. While $[Cu(L1)_2]^+$ is best described as a Cu^I complex with two neutral radical ligands that couple antiferromagnetically, $[Cu(L2)_2]^+$ is a Cu^I complex with two clearly different ligand units in the solid state and with a magnetic susceptibility close to a diamagnetic compound. Further one-electron oxidation of the complex with L1 ligands results in a dication $[Cu(L1)_2]^{2+}$, best described as a Cu^I complex with a twofold oxidised, monocationic ligand and a neutral radical ligand. The stability in at least three redox states, the accumulation of spin density at the ligands and the facile ligand-metal electron transfer make these complexes highly attractive for a variety of applications; here the catalytic aerobic oxidation of alcohols to aldehydes is tested.*

Introduction

The integration of redox-active ligands in molecular coordination compounds leads to intriguing electronic structures and opens up new possibilities for applications in catalysis and materials science.[1–5] Intramolecular ligand-metal electron transfer (IET) processes in these complexes could be used for the activation of substrates in catalytic cycles, with the redox-active ligand acting as electron reservoir; moreover, radical ligands generated by IET generally induce a special ligand-centered reactivity.[6–8] In redox-induced intramolecular electron transfer (RIET) processes, the metal is reduced in an overall oxidation or oxidised in an overall reduction of a coordination compound. The first examples for RIET were reported by Miller et al. for dinuclear cobalt complexes with bridging tetraoxolene ligands.[9–11] With relevance to this work, our group recently reported examples of RIET processes for copper and cobalt complexes with redox-active guanidine ligands.[12,13]

Copper complexes with redox-active ligands were intensively studied.[14–17] A variety of stable Cu^{II} complexes with radical ligands was reported, and phenoxyl radical complexes of salen-type ligands were established as mixed-valent galactose oxidase models.[18–26] The mononuclear complex $Cu^{II}(SQ)_2$ (SQ denotes an *o*-imino-semiquinonato ligand) features two radical ligands. Oxidative addition of bromine leads to a bis(*o*-iminobenzoquinone) complex;[27] the two radical ligands provide the required electrons. Desage-El Murr, Fensterbank et al. reported trifluoromethylation of $Cu^{II}(SQ)_2$[28] and application of the resulting unstable complex as a source of CF_3 radicals.[29] Stoichiometric reactions with aryl boronic acids gave N-arylation products.[30]

We already studied the redox and coordination chemistry of neutral redox-active urea azine ligands.[31–33] Cu^{II} complexes with a neutral, peralkylated urea azine ligand were found to be stable in the solid state, but amenable to IET induced demetallation and decomposition in solution (Scheme 1a).[33] To avoid decomposition, we decided to strengthen the metal-ligand bonding by using anionic urea azine ligands, generated by deprotonation of urea azines with partially alkylated substituents and N-H groups. In this context we note that Panda, Lahiri et al. reported ruthenium complexes of the twice-deprotonated, symmetric thio-urea azine 2,2′-azobis(benzothiazole) (abbt) and found valence tautomerism (VT) between $[\{Ru^{2.5}(acac)_2\}_2(\mu\text{-abbt}^{\bullet-})]$ and $[\{Ru^{III}(acac)_2\}_2(\mu\text{-abbt}^{2-})]$.[34]

Here we report the redox chemistry of the first mononuclear Cu^{II} complexes with two monoanionic, deprotonated urea azine or thio-urea azine ligands, L1 and L2 (Scheme 1b). The formation of complexes with bridging redox-active ligands is avoided by use of asymmetric urea azines or thio-urea azines with only one N-H function. The one-electron oxidation of the initially formed neutral Cu^{II} complexes is accompanied by a RIET process to give unprecedented monocationic Cu^I complexes with oxidised ligands. Further one-electron oxidation is again ligand-centered, leading to a stable dicationic Cu^I complex.

[*] M. Werr, Dr. E. Kaifer, Prof. M. Enders, Prof. H.-J. Himmel
Anorganisch-Chemisches Institut, Ruprecht-Karls Universität Heidelberg
Im Neuenheimer Feld 270, 69120 Heidelberg (Germany)
E-mail: hans-jorg.himmel@aci.uni-heidelberg.de
A. Asyuda, Prof. M. Zharnikov
Angewandte Physikalische Chemie, Ruprecht-Karls Universität Heidelberg
Im Neuenheimer Feld 253, 69120 Heidelberg (Germany)
Supporting information and the ORCID identification number(s) for the author(s) of this article can be found under: https://doi.org/10.1002/anie.202109367.

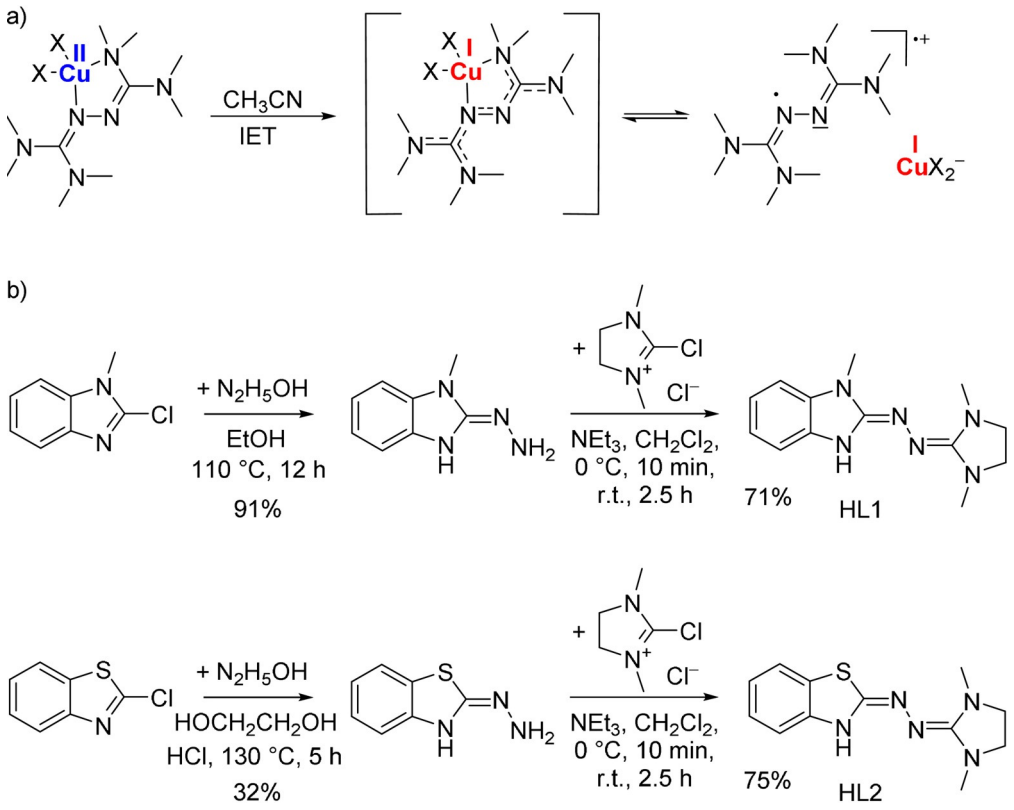

Scheme 1. a) Demetallation of a complex with urea azine ligand initiated by intramolecular electron transfer (IET) from the ligand to the metal (X = Cl, Br). b) Synthesis of asymmetric azines HL1 and HL2.

Results and Discussion

The synthesis of new HL1 and HL2 (protonated versions of the ligands) is sketched in Scheme 1 b, following previously established synthetic strategies by our group.[31,32] Both molecules are built of the same aliphatic guanidinyl group attached to a different aromatic guanidinyl (HL1) or thioguanidinyl (HL2) group. In crystals of HL1, grown by layering a 1,2-difluorobenzene solution with *n*-pentane, dimeric units are formed, in which two molecules are bound by two N-H···N hydrogen bonds (see Supporting Information). B3LYP/def2-TZVP calculations predict a significant binding energy (ΔE including zero-point energy corrections) of 85 kJ mol^{-1} for the dimer. The unit cell contains four different, almost planar molecules. With average values of 1.424 and 1.295 Å, the central N–N single and imino C=N double bond lengths are similar to those in other neutral urea azines.[31,32,33,35]

The redox activity of the protonated ligands was studied by cyclic voltammetry (see Supporting Information). The curve recorded for HL1 contains a relatively sharp oxidation/reduction wave at −0.442 V/−0.545 V and a broad one at 0.102 V/−0.127 V. Similarly, for HL2 a relatively sharp oxidation/reduction wave at −0.235 V/−0.366 V and a broad one at 0.508 V/0.278 V was observed. The underlying two one-electron processes involve a change in the hydrogen bonding or even proton transfer, since hydrogen bonding is strengthened upon oxidation of the hydrogen-bond donor component. The deprotonated versions of the two ligands could adopt three different redox states (anionic, radical neutral or cationic, see Lewis structures in Scheme 2 a).

The two homoleptic Cu^{II} complexes [Cu(L1)$_2$] and [Cu(L2)$_2$] were obtained by reaction of Cu^{II} acetate with HL1 and HL2, respectively, in the presence of KO^{t}Bu (Scheme 2 b). [Cu(L1)$_2$] is more sensitive to dioxygen than [Cu(L2)$_2$]. Structural characterisation in the solid state by SCXRD (Table 1 and Figure 1) found a copper coordination mode in between tetrahedral and square planar with dihedral angles between the two CuN$_2$ planes of 51.5° for [Cu(L1)$_2$] and 54.0° for [Cu(L2)$_2$]. As discussed previously, this special structure is due to σ- and π-contributions of the metal-guanidine bonding.[17] Due to the asymmetric design of the azine ligands, *cis*- or *trans*-type ligand conformations are possible; [Cu(L1)$_2$] crystallises in the *cis*-type and [Cu(L2)$_2$] in the *trans*-type form. The bond parameters (e.g. average Cu-N distance of 1.962 Å in [Cu(L1)$_2$] and 1.965 Å in [Cu(L2)$_2$], and central N–N ligand bond length of 1.426(2) Å in [Cu(L1)$_2$] and 1.420(2) Å in [Cu(L2)$_2$]) are similar for both complexes, indicating Cu^{II} with two monoanionic ligands. We also prepared the zinc complex [Zn(L1)$_2$]. Here, the dihedral angle between the two ZnN$_2$ planes is 79.4°, being closer to the 90° expected for tetrahedral coordination, and the N–N bond length measures 1.432(1) Å.

The UV/Vis spectra of the two neutral complexes (Figure 2 and Supporting Information) are dominated by strong absorptions in the UV region (338 nm, 243 nm for [Cu(L1)$_2$] and 324 nm, 229 nm for [Cu(L2)$_2$]). Only weak bands appear in the visible region (≈450 nm and ≈650 nm for both

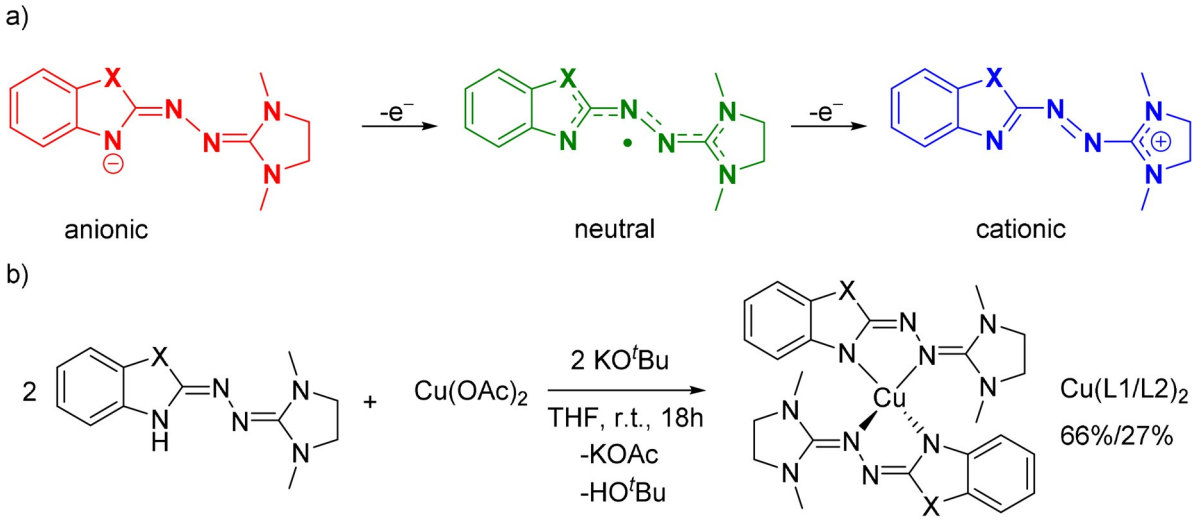

Scheme 2. a) Possible redox states of the new ligands. b) Synthesis of $[Cu(L1)_2]$ and $[Cu(L2)_2]$ (X = NMe (L1) or S (L2)).

Table 1: Structure parameters (bond lengths in Å, angles in °) for all complexes in the solid state from SCXRD.[36]

	$[Zn(L1)_2]$	$[Cu(L1)_2]$	$[Cu(L2)_2]$	$[Cu(L1)_2](SbF_6)$	$[Cu(L2)_2](SbF_6)$
a	1.387(1)	1.381(2)/1.381(2)	1.765(3)	1.376(5)	1.758(3)/1.746(3)
b	1.365(1)	1.371(2)/1.369(2)	1.365(3)	1.343(5)	1.367(4)/1.351(4)
c	1.307(1)	1.305(2)/1.307(2)	1.304(3)	1.340(5)	1.310(4)/1.327(4)
d	1.432(1)	1.426(2)/1.426(2)	1.420(2)	1.369(4)	1.405(4)/1.371(4)
e	1.307(1)	1.313(2)/1.313(2)	1.326(3)	1.341(5)	1.340(4)/1.362(4)
f	1.376(1)	1.362(2)/1.359(2)	1.365(3)	1.342(5)	1.345(4)/1.338(4)
g	1.381(1)	1.381(2)/1.381(2)	1.351(3)	1.368(5)	1.342(4)/1.336(5)
h	1.958(1)	1.924(2)/1.942(2)	1.944(2)	1.933(3)	1.909(3)/1.922(3)
i	2.052(1)	2.007(2)/1.976(2)	1.985(2)	2.095(3)	1.962(3)/1.986(3)
∡ ML_2[a]	79.4°	51.5°	54.0°	65.4°	60.9°

	$[Cu(L1)_2](PF_6)_2$
a	1.348(12)/1.361(11)
b	1.348(12)/1.345(12)
c	1.372(12)/1.355(12)
d	1.348(10)/1.369(10)
e	1.376(12)/1.379(12)
f	1.346(12)/1.325(13)
g	1.332(12)/1.337(12)
h	1.910(8)/1.917(8)
i	1.974(8)/1.981(8)
∡ ML_2[a]	54°

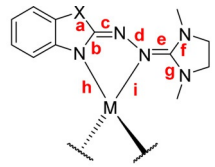

X = NMe: $[Cu(L1)_2]$, $[Zn(L1)_2]$
X = S: $[Cu(L2)_2]$

[a] ML_2 denotes the smallest dihedral angle between the two MN_2 planes.

complexes), being responsible for their green colour. In addition, weak, broad bands around 1900 nm were tentatively assigned to ligand→metal charge transfer excitations. By contrast, the optical spectra for $[Zn(L1)_2]$ (see Supporting Information) showed strong absorption bands only in the UV region (at 337, 284, and 235 nm). In summary, the electron spectra give no hint for the presence of oxidised ligands, in line with the description as Cu^{II} complexes with anionic ligands.

Four one-electron redox processes were found in the cyclic voltammograms of both complexes (Figure 3). The redox potentials are significantly higher (less negative) for $[Cu(L2)_2]$ than for $[Cu(L1)_2]$. The redox process with the lowest potential ($E_{1/2} = -1.40$ V for the redox couple $[Cu(L1)_2]/[Cu(L1)_2]^-$ and -1.29 V for $[Cu(L2)_2]/[Cu(L2)_2]^-$) is assigned to a metal-centered process ($Cu^{II} \rightarrow Cu^{I}$). The potential is too low for a ligand-centered redox event. The low potential of the Cu^{II}/Cu^{I} redox couple for both neutral complexes is in line with the description as Cu^{II} complexes. Then, the second redox process at -0.71 V for $[Cu(L1)_2]^+/[Cu(L1)_2]$ and -0.44 V for $[Cu(L2)_2]^+/[Cu(L2)_2]$ belongs to a ligand-centered redox event ($((L1/L2)^- \rightarrow (L1/L2)^{\bullet 0}$). Two further quasi-reversible, one-electron redox events were observed at $E_{1/2} = -0.27$ and $+0.09$ V for $[Cu(L1)_2]$ and at -0.03 and $+0.31$ V for $[Cu(L2)_2]$. Hence the CV data indicate stability of the complexes in several redox states. However, for $[Cu(L2)_2]$ the waves broaden with increasing scan speed, especially in direction of reduction, arguing for some redox-induced structural and/or electronic changes.

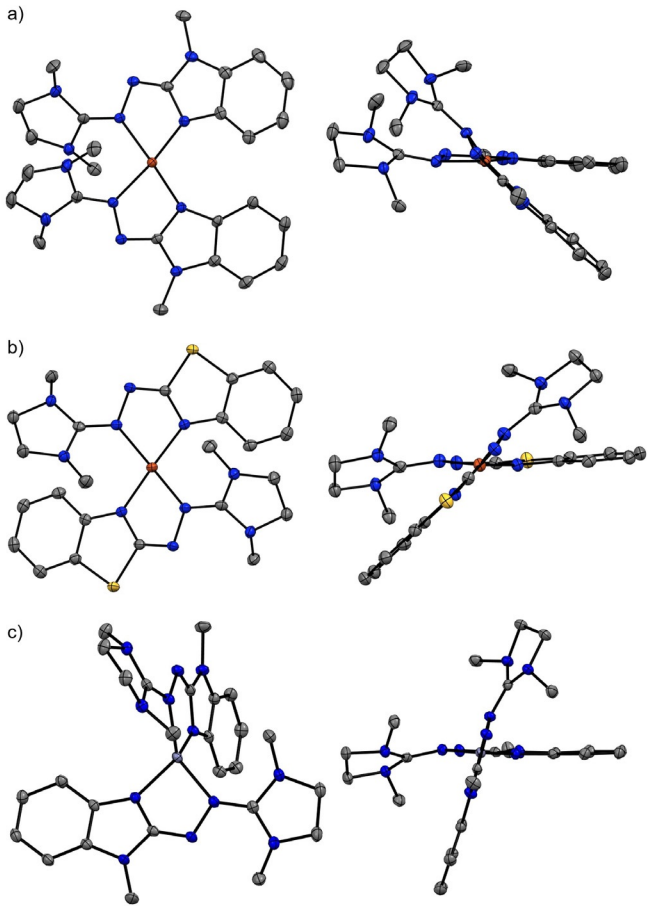

Figure 1. Illustration of the solid-state structures of $[Cu(L1)_2]$ (a), $[Cu(L2)_2]$ (b) and $[Zn(L1)_2]$ (c) from two perspectives. Displacement ellipsoids are drawn at the 50% probability level. Hydrogen atoms are omitted. Colour code: N-blue, C-grey, S-yellow, Cu-red, Zn-silver.

Chemical oxidation of the two complexes with one equivalent of $FcPF_6$ or $AgSbF_6$ (Figure 4a) leads cleanly to the deep-purple salts $[Cu(L1)_2](PF_6/SbF_6)$ and $[Cu(L2)_2](PF_6/SbF_6)$ (83% and 75% isolated yield, respectively). Figure 4b sketches the Lewis structures representing possible descriptions of the charge distributions in $[Cu(L1)_2]^+$ and $[Cu(L2)_2]^+$. Structure $\mathbf{A}^+$ is a Cu^{II} complex with neutral radical and monoanionic ligands. Of course, the unpaired electron could also be delocalised over both ligand units. Structures $\mathbf{B}^+$ and $\mathbf{C}^+$ are Cu^{I} complexes. In $\mathbf{B}^+$, both ligand units are neutral radicals; for $\mathbf{C}^+$ a closed-shell singlet state results with one monocationic and one monoanionic ligand unit. It will be shown in the following that none of the structures alone fits to the analytic data. Structures $\mathbf{B}^+$ and $\mathbf{C}^+$ both contribute to an adequate description of the electronic structure of the monocationic complexes, but the weighting of the two structures is very different for $[Cu(L1)_2]^+$ and $[Cu(L2)_2]^+$. In both cases, oxidation leads to a Cu^{I} complex; overall oxidation induces copper reduction ($Cu^{II} \rightarrow Cu^{I}$) in a redox-induced electron transfer (RIET) process.

SCXRD of both complexes with SbF_6^- counter-ions (crystals obtained by layering saturated 1,2-difluorobenzene solutions with *n*-pentane, Figure 4c and Table 1), showed that the two ligands are equal in $[Cu(L1)_2]^+$, but significantly different in $[Cu(L2)_2]^+$. In both cases, the central N–N bond is shortened upon oxidation, from 1.426(2) Å in $[Cu(L1)_2]$ to 1.369(4) Å in $[Cu(L1)_2]^+$, and from 1.420(2) Å in $[Cu(L2)_2]$ to 1.405(4)/1.371(4) Å in $[Cu(L2)_2]^+$. By contrast, the two imino N=C bonds in the neutral complexes (1.305(2)/1.307(2)/1.313(2)/1.313(2) Å and 1.304(3)/1.326(3) Å in $[Cu(L1)_2]$ and $[Cu(L2)_2]$, respectively), are elongated (to 1.340(5)/1.341(5) Å and 1.310(4)/1.327(4)/1.340(4)/1.362(4) Å in $[Cu(L1)_2]^+$ and $[Cu(L2)_2]^+$, respectively). The average Cu–N bond length and the dihedral angle increase upon oxidation of $[Cu(L1)_2]$, clearly signalling formation of a Cu^{I} complex with two neutral radical ligands ($\mathbf{B}^+$ in Figure 4b). In the case of $[Cu(L2)_2]^+$, the differences in the ligand structures are far too large to be explained by crystal packing effects, pointing to different ligand redox states. With 1.405(4) and 1.371(4) Å, the N–N bond lengths are both shorter than in neutral $[Cu(L2)_2]$ (1.420(2) Å). The Cu–N bond distances vary (1.909(3)/1.922(3) Å resp. 1.962(3)/1.986(3) Å) and oxidation leads to an increase of the dihedral angle at the copper atom (from 54.0° in $[Cu(L2)_2]$ to 60.9° in $[Cu(L2)_2]^+$), pointing again to Cu^{I}. The structure indicates a significant contribution of $\mathbf{C}^+$. Structure $\mathbf{A}^+$ cannot be completely discarded at this point of the discussion, but is not in line with the results of the other analytic data (see below).

The UV/Vis spectra of $[Cu(L1)_2]^+$ and $[Cu(L2)_2]^+$ show intense absorptions in the vis region, but at different wavelengths, viz. 505 and 555 nm (shoulder) for $[Cu(L1)_2]^+$ and 485 and 720 nm (shoulder) for $[Cu(L2)_2]^+$ (Figure 2a and Supporting Information), pointing to the presence of oxidised ligands. The simulated electron spectrum for the isolated neutral radical L1$^{\bullet}$ based on TD-DFT calculations (B3LYP + D3/def2-TZVP, Figure 2c) closely matches the experimental spectrum of $[Cu(L1)_2]^+$ in the visible region, supporting description $\mathbf{B}^+$ for $[Cu(L1)_2]^+$. The differences in the electron spectra of the two complexes point to different ligand redox states, in line with a significant contribution from $\mathbf{C}^+$ in the case of $[Cu(L2)_2]^+$.

Background-corrected Cu 2p X-ray photoelectron (XP) spectra of the complexes $[Cu(L1)_2]PF_6$ and $[Cu(L2)_2]PF_6$ are shown in Figure 5; complementary C 1s, N 1s, and S 2p XP data are presented in Supporting Information. Note that the wide scan spectra of both complexes (not shown) exhibit a pronounced F 1s peak, manifesting the expected presence of fluorine in the counter ions. The Cu 2p XP spectra in Figure 5 exhibit the Cu $2p_{3/2}$ and Cu $2p_{1/2}$ components at binding energies of 932.8 eV and 952.6 eV for complex $[Cu(L1)_2]PF_6$ and 932.6 and 952.8 eV for $[Cu(L2)_2]PF_6$. These energies are characteristic of copper in the oxidation state +1,[37] corresponding to the electronic configuration $3d^{10}$.[38] The Cu $2p_{3/2}$ and Cu $2p_{1/2}$ components represent well-defined singular peaks, with no traces of the analogous components characteristic of copper in the oxidation state +2, expected at a binding energy of 934.3–934.7 eV for Cu $2p_{3/2}$ ($3d^9$ configuration).[39] The spectrum of the latter species is also characterized by the intense satellite structure in the post-peak region,[39,40] fully absent in the spectra presented in Figure 5. Hence the XPS data clearly show that $[Cu(L1)_2]^+$ and $[Cu(L2)_2]^+$ are Cu^{I} complexes.

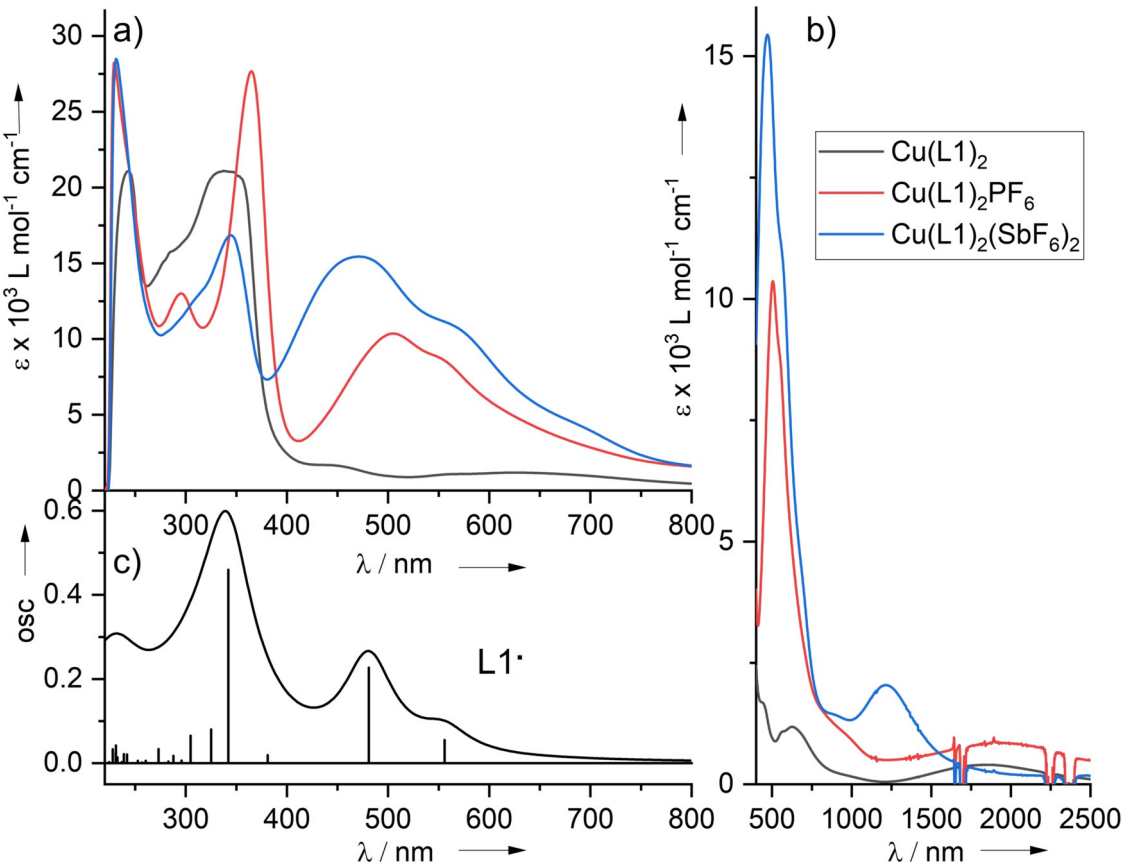

Figure 2. a) UV/Vis spectra of $[Cu(L1)_2]$, $[Cu(L1)_2]^+$ and $[Cu(L1)_2]^{2+}$ in CH_2Cl_2. b) Zoom into the visible and near-IR regions. c) Simulation of the electron spectrum of the free radical L1• from TD-DFT (B3LYP + D3/def2-TZVP) calculations.

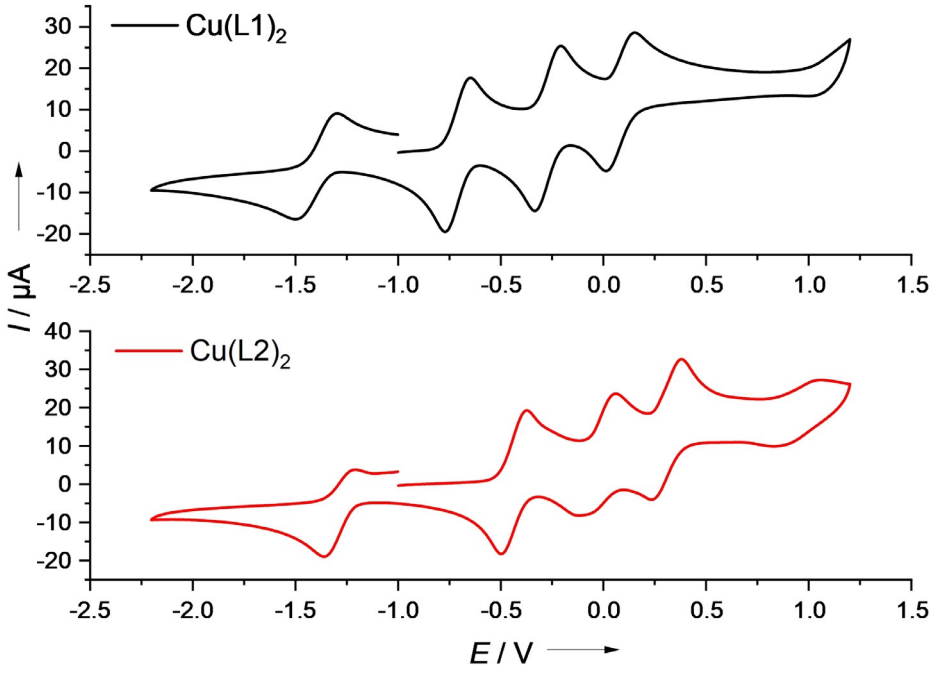

Figure 3. Cyclic voltammograms for $[Cu(L1)_2]$ and $[Cu(L2)_2]$ in CH_2Cl_2 (100 mVs^{-1} scan rate, 0.1 M nBu_4NPF_6 as supporting electrolyte, potentials given vs. Fc^+/Fc).

Magnetometric (SQUID) measurements on a solid powder sample of $[Cu(L1)_2](SbF_6)$ confirmed the presence of two unpaired electrons (Figure 6), in accordance with $\mathbf{B}^+$ (Figure 4b). A curve typical of a weakly antiferromagnetically coupled two-spin system was obtained, and an isotropic J value of $-3.5\ cm^{-1}$ (spin Hamiltonian $H = -J\ S_1\ S_2$) and a g factor of 1.9947 followed from a Bleaney–Bowers curve fit. The magnetometric measurements on $[Cu(L2)_2]SbF_6$ gave different results. Here the χT value is small, arguing for structure $\mathbf{B}^+$ with an extremely strong antiferromagnetic coupling between the two ligand-centered unpaired electrons or (more likely) a dominating contribution from the closed-shell structure $\mathbf{C}^+$ in the solid state, the latter being in line with the presence of two different ligands in the XRD structure.

Paramagnetic NMR spectroscopy has been established as a powerful tool for the analysis of paramagnetic molecules in solution;[41,42] we applied this technique previously for

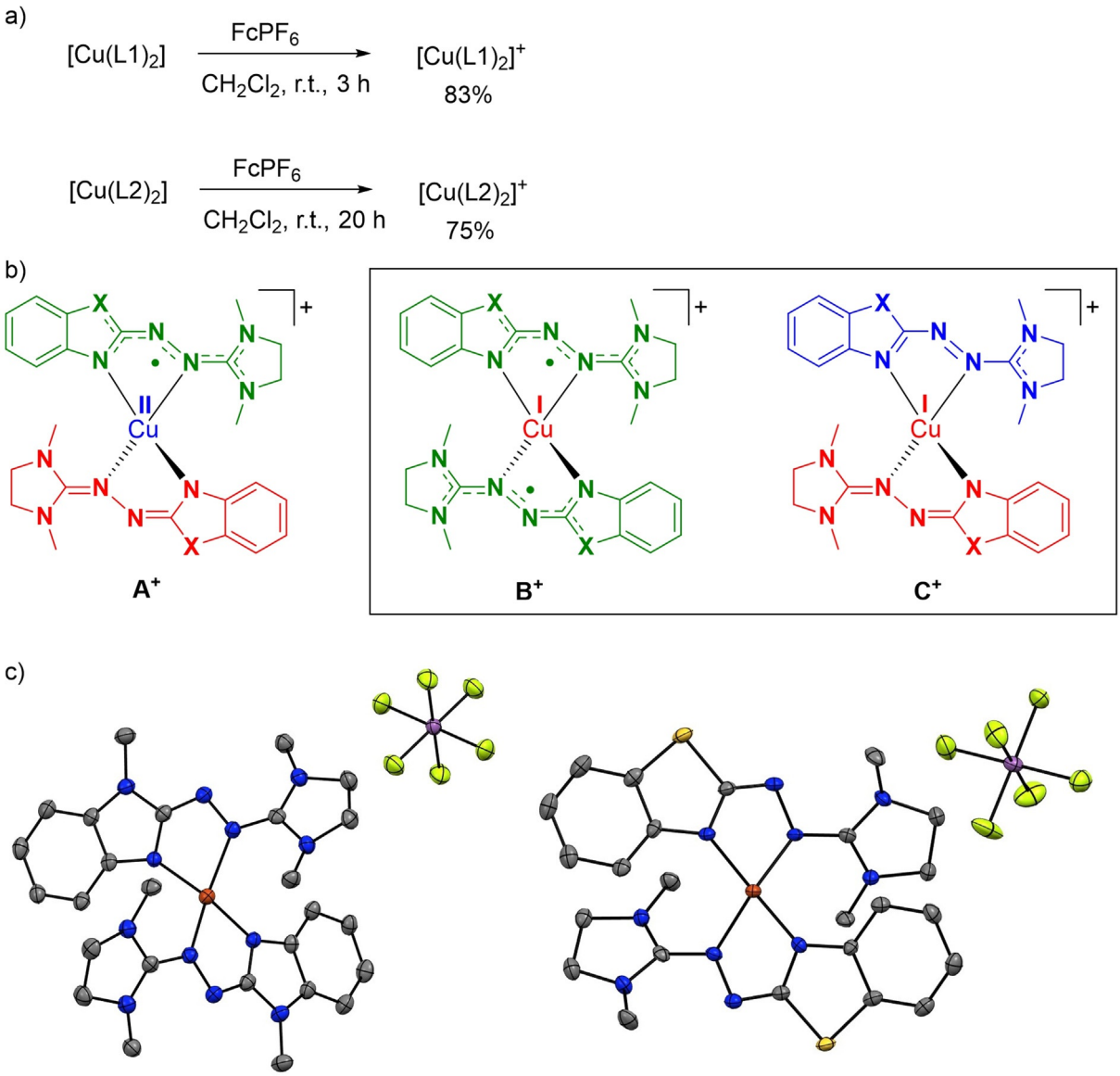

Figure 4. a) One-electron oxidation of the neutral complexes. b) Possible descriptions of the electronic distribution in $[Cu(L1)_2]^+$ and $[Cu(L2)_2]^+$. Structures $\mathbf{B}^+$ and $\mathbf{C}^+$ describe best the electronic structures. c) Illustration of the solid-state structures of $[Cu(L1)_2](SbF_6)$ (left) and $[Cu(L2)_2](SbF_6)$ (right). Displacement ellipsoids are drawn at the 50% probability level. Hydrogen atoms are omitted. Colour code: N-blue, C-grey, S-yellow, Cu-red, Sb-mauve, F-green.

complexes with guanidine ligands.[43–45] Figure 7 shows the ^{1}H NMR spectra for $[Cu(L1)_2]^+$ and $[Cu(L2)_2]^+$ at various temperatures (see ^{13}C NMR spectra in the Supporting Information). The signal dispersion is much larger for $[Cu(L1)_2]^+$, indicating more spin density on the ligands. Seven signals are observed at high temperature corresponding to four aromatic, two methyl and one methylene hydrogen signal. The latter corresponds to four inequivalent H atoms which are in a fast chemical exchange (diastereotopic H atoms of each CH_2 group and inequivalence of the two CH_2 groups due to restricted rotation around the C=N double bond). At lower temperatures, this signal splits into two and then into four signals. The equivalence of the hydrogen atoms of the ethylene bridge stems from two dynamic processes. One process interconverts the carbon atoms by a rotation around the N=C double bond; a second dynamic process exchanges the diastereotopic H atoms of each CH_2 moiety (see Supporting information).

The ^{1}H NMR spectrum of $[Cu(L2)_2]^+$ could be assigned similar to that of $[Cu(L1)_2]^+$, but the smaller signal dispersion indicates less spin density on the ligands. The aromatic protons give rise to the two downfield shifted signals at $\delta =$ 18.12 and 11.54 ppm as well as to the two upfield shifted signals at $\delta = -16.23$ and -24.84 ppm. Also, the NCH_3 groups at the aliphatic guanidinyl moiety are chemically equivalent in the NMR spectrum and likely belong to the downfield shifted signal at $\delta = 21.80$ ppm. In difference to the spectra of $[Cu(L1)_2]^+$, the CH_2 protons give rise to two signals at room temperature, however 2D NOESY experiments show that they are in a chemical exchange.

The temperature-dependence of the NMR signals deviates for both complexes from the Curie behaviour ($1/T$

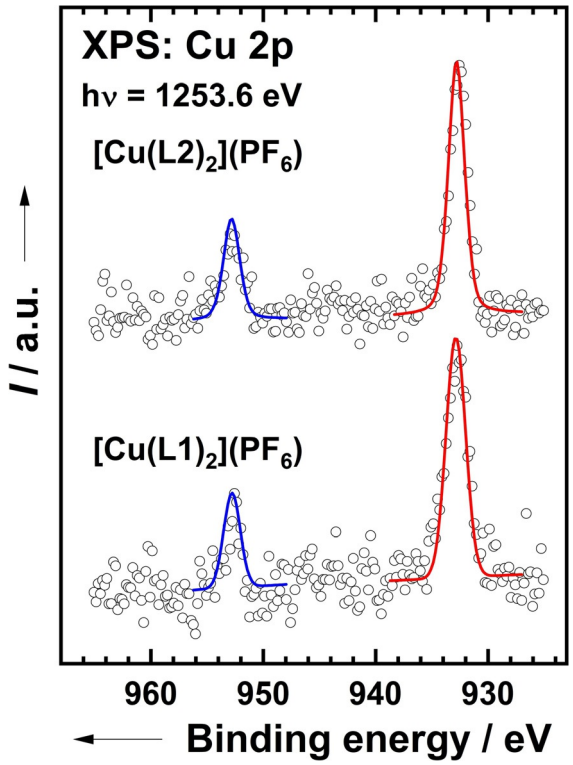

Figure 5. Background-corrected Cu 2p XP spectra of $[Cu(L1)_2]PF_6$ and $[Cu(L2)_2]PF_6$ (open circles). The Cu $2p_{3/2}$ and Cu $2p_{1/2}$ components are tentatively fitted by symmetric Voigt peaks (solid red and blue lines, respectively).

dependence) which is expected for the Fermi contact shift for non-coupled systems; the signals for both complexes tend to shift into the diamagnetic region with decreasing temperature. It was not possible to fit adequately the NMR data of $[Cu(L1)_2]^+$ (see Supporting Information) with the standard formula for a magnetically-coupled system with two spin centers $S_A = S_b = 1/2$.[46] The data at low and high temperatures seem to follow different functions. On the other hand, fits of the temperature-dependence of the NMR signals of $[Cu(L2)_2]^+$ were satisfactory, but only with extraordinary large hyperfine coupling constants A and extremely large antiferromagnetic coupling constant *J* as fit parameters (see Supporting Information). The NMR data are in line with a mixture of two different descriptions of the charge distribution, with a larger contribution of $\mathbf{C}^+$ to the electronic structure in the case of $[Cu(L2)_2]^+$.

In summary, all results, especially SCXRD, UV/Vis and XP spectroscopy, and also EPR spectroscopy (main signal contribution with *g* factor near the free-electron value, only weak copper hyperfine structure visible due to small amount of copper-centered spin density (see Supporting Information)) indicate that $[Cu(L1)_2]^+$ and $[Cu(L2)_2]^+$ are both Cu^I complexes with two oxidised ligand units. For $[Cu(L1)_2]^+$, the electronic structure is best described by $\mathbf{B}^+$ in Figure 4b (being in pleasing agreement with the SCXRD and SQUID results), but the difficulties in fitting the temperature-dependence of the NMR signals argues for a (temperature-dependent) contribution of $\mathbf{C}^+$ or alternatively to a sensitivity of the electronic structure to the discussed dynamic effects in solution. In the case of $[Cu(L2)_2]^+$, the inequivalence of the two ligand units in the solid-state structure and the low χT value clearly point to a larger contribution from structure $\mathbf{C}^+$ with respect to $[Cu(L1)_2]^+$. However, the NMR data show some paramagnetic character, in line with a significant contribution from structure $\mathbf{B}^+$. A conversion from $\mathbf{B}^+$ to $\mathbf{C}^+$ could be described as a ligand disproportionation. Interestingly, Chaudhuri, Wieghardt et al. reported a Zn complex with two redox-active ligands for which the presence of two isomers related by such a ligand disproportionation was indeed evidenced.[47] The green diamagnetic form of this complex is thermodynamically more stable than the red paramagnetic isomer. The authors demonstrate that isomerisation from the red, paramagnetic form to the green, diamagnetic isomer could be initiated by redox cycling or changes in the solvent or experimental conditions. In the case of $[Cu(L2)_2]^+$,

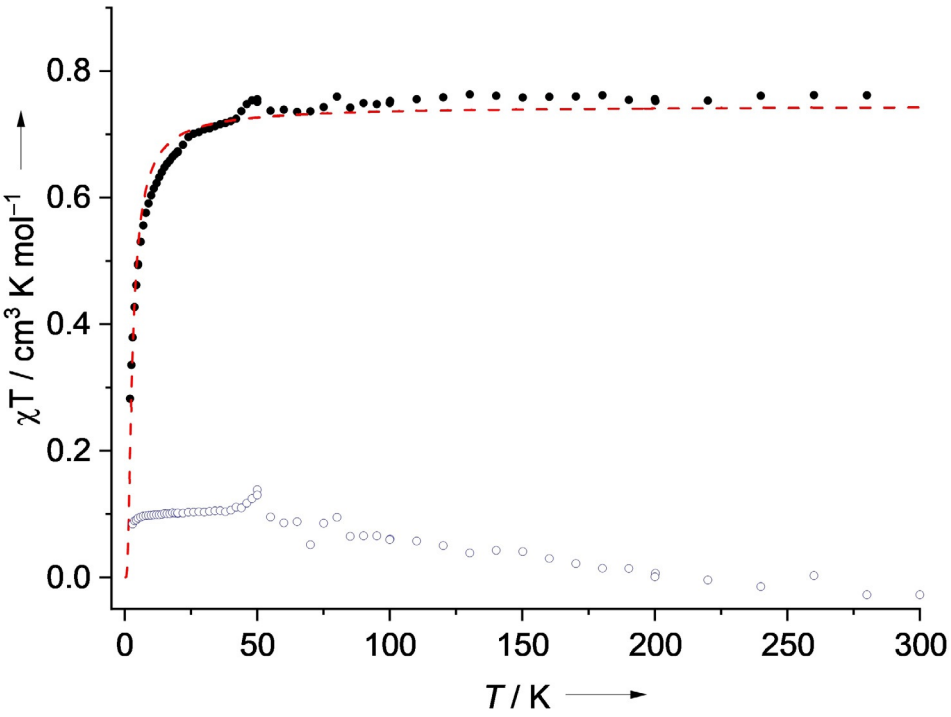

Figure 6. Plot of the magnetometric (SQUID) data for $[Cu(L1)_2](SbF_6)$ (black filled circles) and $[Cu(L2)_2](PF_6)$ (blue open circles), measured at 50 mT. The dashed red curve results from a Bleaney–Bowers fit for $[Cu(L1)_2]SbF_6$.

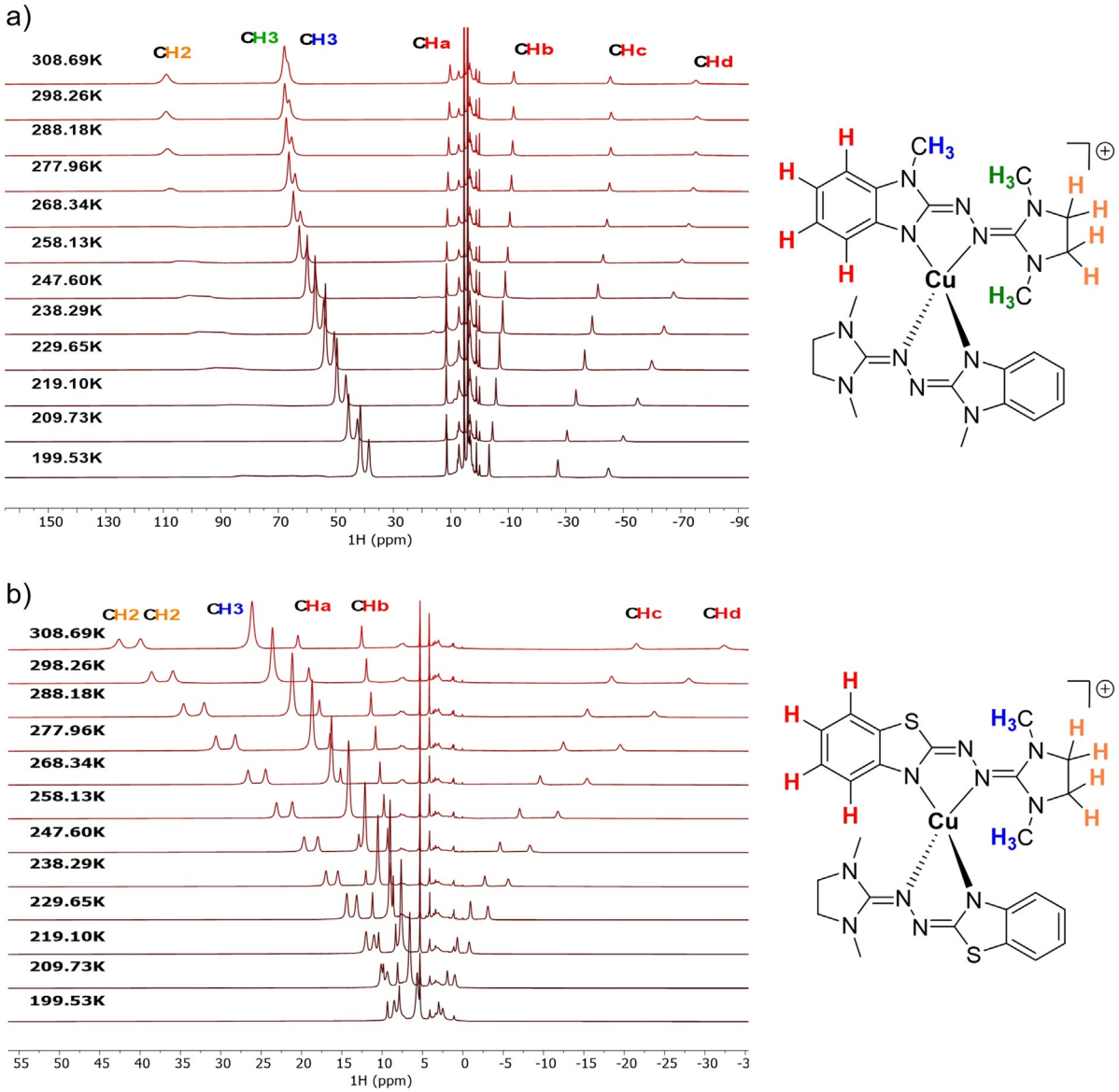

Figure 7. Paramagnetic ^{1}H NMR spectra of a) $[Cu(L1)_2]PF_6$ and b) $[Cu(L2)_2]PF_6$ at various temperatures in CD_2Cl_2 (399.89 MHz).

the electronic structure certainly differs in solution and in the solid state. However, we have no indication for the co-existence of two isomers (one being closer to structure $\mathbf{C}^+$ and the other one closer to $\mathbf{B}^+$) or the possibility to initiate isomerisation by change of solvent or reaction conditions.

The RIET process could be roughly rationalized as follows. The +II oxidation state of the copper atom in neutral $[Cu(L1)_2]$ and $[Cu(L2)_2]$ is certainly favoured by a significant ionic contribution to bonding between the anionic ligands and Cu^{II}. Ligand-centered one-electron oxidation generating a neutral radical ligand decreases this ionic contribution, thereby destabilising Cu^{II} with respect to Cu^{I}. In the case of $[Cu(L1)_2]^+$, an electron is transferred from the second ligand to copper, leading eventually to a Cu^{I} complex with two neutral radical ligands (structure $\mathbf{B}^+$). For $[Cu(L2)_2]^+$, the electron needed for copper reduction stems in part from the neutral radical ligand. It should be noted that Cu^{I} complexes with two radical ligand units like $[Cu(L1)_2]^+$ are extremely rare and almost exclusively restricted to a few complexes with two verdazyl radical ligands.[48–53] Interestingly, the singlet-triplet energy difference in these systems could be tuned and strongly depends on the coordination mode.

Further one-electron oxidation of $[Cu(L1)_2](SbF_6)$ with a second equivalent of $AgSbF_6$ produced the salt of the dicationic complex, $[Cu(L1)_2](SbF_6)_2$ in 58% isolated yield (Figure 8a). This complex could either be described as a Cu^{II} complex with two neutral radical ligands ($\mathbf{A}^{2+}$), summing up to three unpaired electrons, as a Cu^{I} complex with a cationic ligand and a neutral radical ligand ($\mathbf{B}^{2+}$) or a Cu^{II} complex with one anionic ligand and one cationic ligand ($\mathbf{C}^{2+}$), resulting in one unpaired electron for the latter two (Figure 8b). Obviously, the electronic structure could also be in between these three descriptions. XRD of crystals of $[Cu(L1)_2](PF_6)_2$, obtained from gas-phase diffusion of *n*-pentane into a saturated acetone solution (Table 1 and Figure 8c),

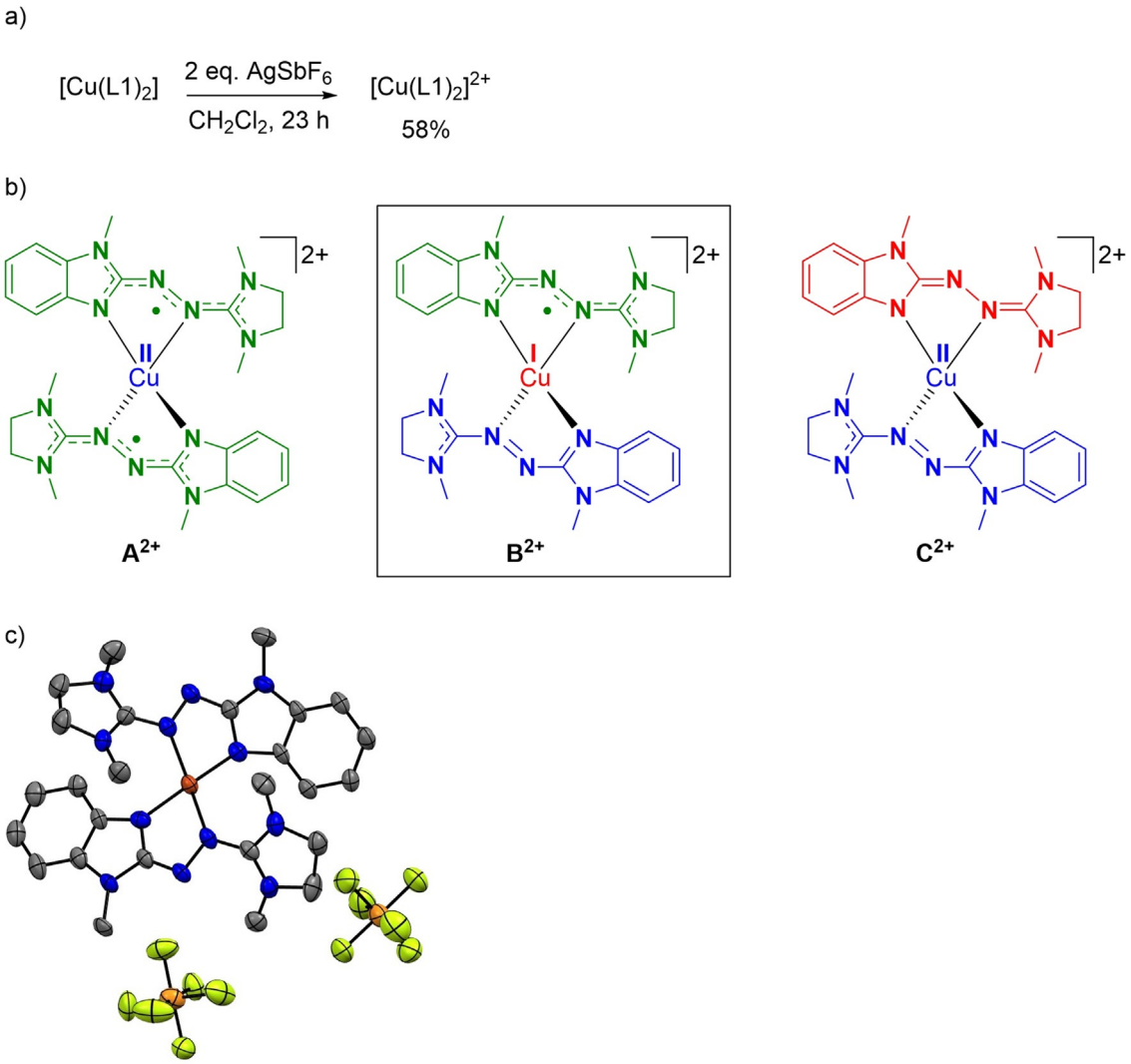

Figure 8. a) Two-electron oxidation of $[Cu(L1)_2]$. b) Possible electronic structures of $[Cu(L1)_2]^{2+}$. Structure $\mathbf{B}^{2+}$ in the box describes best the electronic structure. c) Illustration of the solid-state structure of $[Cu(L1)_2](PF_6)_2$ (without co-crystallised acetone). Displacement ellipsoids are drawn at the 50% probability level. Hydrogen atoms are omitted. Colour code: N-blue, C-grey, Cu-red, P-orange, F-green.

showed that the two ligand units are slightly different. The N–N bonds of the ligands measure 1.348(10) and 1.369(10) Å.

In the UV/Vis spectrum of $[Cu(L1)_2]^{2+}$ (see Figure 2), strong absorptions appear in the visible region (at 568 nm (sh) and 471 nm), being close to the absorptions in the monocationic complex $[Cu(L1)_2]^{+}$ (555 nm (sh) and 505 nm). In addition, a quite strong band appears in the NIR region near 1200 nm, tentatively assigned to a metal→ligand charge-transfer transition. These bands strongly argue for a neutral radical ligand unit, as present in $\mathbf{B}^{2+}$.

Magnetometric (SQUID) measurements on a solid powder sample of $[Cu(L1)_2](SbF_6)_2$ (see Supporting Information) show that with increasing temperature the χT value approaches the expectation value for one unpaired electron (0.375 $cm^3 K mol^{-1}$). It drops down at very low temperatures (ca. 25 K), most likely due to intermolecular antiferromagnetic coupling. Hence these data strongly support structure $\mathbf{B}^{2+}$. They are clearly not compatible with $\mathbf{A}^{2+}$.

EPR spectra in CH_2Cl_2 (see Supporting Information) at room-temperature show a single signal with a *g* value of 2.004, compatible with a ligand-centered radical but not with a copper-centered radical (in the latter case the *g* value should be higher). Hence, all results indicate that $\mathbf{B}^{2+}$ describes the electronic structure most adequately. Structure $\mathbf{B}^{2+}$ directly follows from ligand-centered one-electron oxidation of $[Cu(L1)_2]^{+}$ (Cu^{I} complex with two neutral radical ligands).

Finally, we tested the catalytic performance of the new complexes in the aerobic alcohol oxidation to aldehydes. Benzyl alcohol (BzOH) and cinnamyl alcohol (CinnOH) were used as model substrates. The best results with BzOH (Table 2) were obtained with 5 mol% of the catalyst and 2 equiv. of Cs_2CO_3 (93% conversion for $[Cu(L1)_2]$ as catalyst in C_7D_8, and 99% for $[Cu(L2)_2]$ as catalyst in CD_2Cl_2). By contrast, $[Zn(L1)_2]$ was only poorly active (entry 15). Oxidation of CinnOH under the optimized conditions yielded 72%

Table 2: Summary of the results of the catalytic experiments.

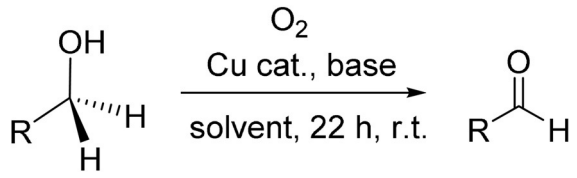

Entry	Catalyst	Cat. mol%	Base	Base eq	Solvent	Substrate	Conversion/%
1	$[Cu(L1)_2]$	5	Cs_2CO_3	2	CD_2Cl_2	BzOH	87
2	$[Cu(L1)_2]$	1	Cs_2CO_3	2	CD_2Cl_2	BzOH	62
3	$[Cu(L1)_2]$	5	Cs_2CO_3	2	Tol-d8	BzOH	93
4	$[Cu(L1)_2]$	5	Cs_2CO_3	2	CD_3CN	BzOH	80
5	$[Cu(L1)_2]$	5	Cs_2CO_3	1	CD_2Cl_2	BzOH	65
6	$[Cu(L1)_2]$	5	Cs_2CO_3	0.1	CD_2Cl_2	BzOH	29
7	$[Cu(L1)_2]$	5	no Base	0	CD_2Cl_2	BzOH	29
8	$[Cu(L1)_2]$	5	KOH	2	CD_2Cl_2	BzOH	10
9	$[Cu(L2)_2]$	5	Cs_2CO_3	2	CD_2Cl_2	BzOH	99
10	$[Cu(L2)_2]$	2	Cs_2CO_3	2	CD_2Cl_2	BzOH	98
11	$[Cu(L2)_2]$	1	Cs_2CO_3	2	CD_2Cl_2	BzOH	54
12	$[Cu(L2)_2]$	5	Cs_2CO_3	2	Tol-d8	BzOH	93
13	$[Cu(L2)_2]$	5	Cs_2CO_3	2	CD_2Cl_2	CinnOH	72
14	$[Cu(L2)_2]$	5	Cs_2CO_3	2	CD_2Cl_2	nOctOH	2
15	$[Zn(L1)_2]$	5	Cs_2CO_3	2	Tol-d8	BzOH	17

*NMR conversion determined from substrate/product ratio.

conversion. On the other hand, the oxidation of the primary alcohol *n*OctOH failed (entry 14). Signals due to the urea 1,3-dimethyl-2-imidazolidinone were observed in the NMR spectra after 22 h reaction time, and traces of hydrazone in the reactions with $[Cu(L2)_2]$ as catalyst. The slow catalyst deactivation by decomposition with increasing reaction time explains the reduced conversion with a lower catalyst loading of 1 mol% (entry 2). In this respect, the new catalysts behave similar to previously reported catalysts.[19,20,24,25,54] Additional experiments (see Supporting Information) indicate that the catalytic activity (conversion/time) of the two complexes is comparable within the first 5 h of reaction. Interestingly, a higher conversion is eventually achieved with $[Cu(L2)_2]$, although L1 is a better electron-donor than L2 (Table 2). Complex $[Cu(L1)_2]$ is more rapidly oxidised by dioxygen and seems to decompose more rapidly in high oxidation states. Moreover, "overoxidation" of this complex (removal of three electrons) due to the lower redox potentials for all three one-electron oxidation steps (see CV curves in Figure 3) possibly leads to an increased loss of the catalyst. Further analysis of the catalytic mechanism is the subject of ongoing research in our laboratory.

Conclusion

New homoleptic Cu^{II} complexes $[Cu(L1)_2]$ and $[Cu(L2)_2]$ with monoanionic, redox-active and asymmetric ligands (urea azines (L1) or thio-urea azines (L2)) were synthesised. The ligand design relied on previously established procedures by our group for the directed synthesis of asymmetric redox-active urea azines and related thio-urea azines. Only by virtue of their asymmetric structure, these ligands could be used after deprotonation as chelating, anionic redox-active ligands for mononuclear complexes. In chemical redox reactions, the monocationic complexes $[Cu(L1)_2]^+$ and $[Cu(L2)_2]^+$ as well as the dicationic complex $[Cu(L1)_2]^{2+}$ were synthesised and fully characterized. Fortunately, the electronic structure elucidation, relying on a variety of different analytical methods, is facilitated by structural characterisation in three different redox states, being extremely rare in the field of complexes with redox-active ligands.

One-electron oxidation of $[Cu(L1)_2]$ and $[Cu(L2)_2]$ is accompanied by an unprecedented RIET process leading to metal reduction (Cu^{II}—Cu^{I}) upon overall one-electron oxidation. In $[Cu(L1)_2]^+$, the Cu^{I} center is coordinated by two equivalent, neutral radical ligands, that couple antiferromagnetically. In $[Cu(L2)_2]^+$, the Cu^{I} atom is coordinated by two different ligands, resulting in a complex with a magnetic susceptibility close to a diamagnetic compound. Hence slight variations within the ligand design lead to significant changes in the electronic structure and properties.

The dication $[Cu(L1)_2]^{2+}$ was synthesised by two-electron oxidation of $[Cu(L1)_2]$. In the solid-state structure, the two ligand units are different, and a detailed analysis indicates that the electronic structure is best described in terms of a Cu^{I} complex with one twofold-oxidised monocationic ligand unit and one singly-oxidised neutral radical ligand.

Their exceptional stability in several redox states makes complexes of redox-active asymmetric azine ligands highly interesting for applications. Within a representative test reaction, their use for the catalytic aerobic oxidation of alcohols to aldehydes was demonstrated. In ongoing work, we explore further catalysis with copper, and also zinc and cobalt complexes of these novel ligand platforms.

Acknowledgements

The authors gratefully acknowledge continuous financial support by the German research foundation (DFG). We thank the state of Baden-Württemberg through bwHPC and the German Research Foundation (DFG) through grant no INST 40/575-1 FUGG (JUSTUS 2 cluster). A.A. acknowledges the financial support by the DAAD-ACEH Scholarship of Excellence. Open Access funding enabled and organized by Projekt DEAL.

Conflict of Interest

The authors declare no conflict of interest.

Keywords: alcohol oxidation · copper · radicals · redox-induced electron transfer · urea azines

[1] W. I. Dzik, J. I. van der Vlugt, J. N. H. Reek, B. de Bruin, *Angew. Chem. Int. Ed.* **2011**, *50*, 3356 – 3358; *Angew. Chem.* **2011**, *123*, 3416 – 3418.
[2] J. I. van der Vlugt, *Eur. J. Inorg. Chem.* **2012**, 363 – 375.
[3] D. L. J. Broere, R. Plessius, J. I. van der Vlugt, *Chem. Soc. Rev.* **2015**, *44*, 6886 – 6915.
[4] A. Das, C. Hessin, Y. Ren, M. Desage-El Murr, *Chem. Soc. Rev.* **2020**, *49*, 8840 – 8867.
[5] N. P. van Leest, F. J. de Zwart, M. Zhou, B. de Bruin, *JACS Au* **2021**, *1*, 1101 – 1115.
[6] J. Jacquet, M. Desage-El Murr, L. Fensterbank, *ChemCatChem* **2016**, *8*, 3310 – 3316.
[7] A. I. O. Suarez, V. Lyaskovskyy, J. N. H. Reek, J. I. van der Vlugt, B. de Bruin, *Angew. Chem. Int. Ed.* **2013**, *52*, 12510 – 12529; *Angew. Chem.* **2013**, *125*, 12740 – 12760.
[8] J. I. van der Vlugt, *Chem. Eur. J.* **2019**, *25*, 2651 – 2662.
[9] K. S. Min, A. G. DiPasquale, J. A. Golen, A. L. Rheingold, J. S. Miller, *J. Am. Chem. Soc.* **2007**, *129*, 2360 – 2368.
[10] K. S. Min, A. G. DiPasquale, A. L. Rheingold, H. S. White, J. S. Miller, *J. Am. Chem. Soc.* **2009**, *131*, 6229 – 6236.
[11] J. S. Miller, K. S. Min, *Angew. Chem. Int. Ed.* **2009**, *48*, 262 – 272; *Angew. Chem.* **2009**, *121*, 268 – 278.
[12] D. F. Schrempp, E. Kaifer, H. Wadepohl, H.-J. Himmel, *Chem. Eur. J.* **2016**, *22*, 16187 – 16199.
[13] L. Lohmeyer, F. Schön, E. Kaifer, H.-J. Himmel, *Angew. Chem. Int. Ed.* **2021**, *60*, 10415 – 10422; *Angew. Chem.* **2021**, *133*, 10506 – 10514.
[14] A. Das, Y. Ren, C. Hessin, M. Desage-El Murr, *Beilstein J. Org. Chem.* **2020**, *16*, 858 – 870.
[15] J. Jacquet, K. Cheaib, Y. Ren, H. Vezin, M. Orio, S. Blanchard, L. Fensterbank, M. Desage-El Murr, *Chem. Eur. J.* **2017**, *23*, 15030 – 15034.
[16] H.-J. Himmel, *Z. Anorg. Allg. Chem.* **2013**, *639*, 1940 – 1952.
[17] H.-J. Himmel, *Inorg. Chim. Acta* **2018**, *481*, 56 – 68.
[18] J. Müller, T. Weyhermüller, E. Bill, P. Hildebrandt, L. Ould-Moussa, T. Glaser, K. Wieghardt, *Angew. Chem. Int. Ed.* **1998**, *37*, 616 – 619; *Angew. Chem.* **1998**, *110*, 637 – 640.
[19] P. Chaudhuri, M. Hess, T. Weyhermüller, K. Wieghardt, *Angew. Chem. Int. Ed.* **1999**, *38*, 1095 – 1098; *Angew. Chem.* **1999**, *111*, 1165 – 1168.
[20] P. Chaudhuri, M. Hess, J. Müller, K. Hildenbrand, E. Bill, T. Weyhermüller, K. Wieghardt, *J. Am. Chem. Soc.* **1999**, *121*, 9599 – 9610.
[21] K. Parikka, E. Master, M. Tenkanen, *J. Mol. Catal. B* **2015**, *120*, 47 – 59.
[22] C. T. Lyons, T. D. P. Stack, *Coord. Chem. Rev.* **2013**, *257*, 528 – 540.
[23] R. C. Pratt, T. D. P. Stack, *J. Am. Chem. Soc.* **2003**, *125*, 8716 – 8717.
[24] S. E. Balaghi, E. Safaei, L. Chiang, E. W. Y. Wong, D. Savard, R. M. Clarke, T. Storr, *Dalton Trans.* **2013**, *42*, 6829 – 6839.
[25] Z. Alaji, E. Safaei, L. Chiang, R. M. Clarke, C. Mu, T. Storr, *Eur. J. Inorg. Chem.* **2014**, 6066 – 6074.
[26] M. Orio, O. Jarjayes, H. Kanso, C. Philouze, F. Neese, F. Thomas, *Angew. Chem. Int. Ed.* **2010**, *49*, 4989 – 4992; *Angew. Chem.* **2010**, *122*, 5109 – 5112.
[27] C. Mukherjee, T. Weyhermüller, E. Bothe, P. Chaudhuri, *Inorg. Chem.* **2008**, *47*, 2740 – 2746.
[28] J. Jacquet, E. Salanouve, M. Orio, H. Vezin, S. Blanchard, E. Derat, M. Desage-El Murr, L. Fensterbank, *Chem. Commun.* **2014**, *50*, 10394 – 10397.
[29] J. Jacquet, S. Blanchard, E. Derat, M. Desage-El Murr, L. Fensterbank, *Chem. Sci.* **2016**, *7*, 2030 – 2036.
[30] J. Jacquet, P. Chaumont, G. Gontard, M. Orio, H. Vezin, S. Blanchard, M. Desage-El Murr, L. Fensterbank, *Angew. Chem. Int. Ed.* **2016**, *55*, 10712 – 10716; *Angew. Chem.* **2016**, *128*, 10870 – 10874.
[31] H. Herrmann, M. Reinmuth, S. Wiesner, O. Hübner, E. Kaifer, H. Wadepohl, H.-J. Himmel, *Eur. J. Inorg. Chem.* **2015**, 2345 – 2361.
[32] M. Werr, E. Kaifer, H. Wadepohl, H.-J. Himmel, *Chem. Eur. J.* **2019**, *25*, 12981 – 12990.
[33] H. Herrmann, E. Kaifer, H.-J. Himmel, *Chem. Eur. J.* **2017**, *23*, 5520 – 5528.
[34] A. Singh, S. Panda, S. Dey, G. K. Lahiri, *Angew. Chem. Int. Ed.* **2021**, *60*, 11206 – 11210; *Angew. Chem.* **2021**, *133*, 11306 – 11310.
[35] M. Reinmuth, C. Neuhäuser, P. Walter, M. Enders, E. Kaifer, H.-J. Himmel, *Eur. J. Inorg. Chem.* **2011**, 83 – 90.
[36] Deposition Numbers 2092840 (for L1H), 2092838 (for [Cu(L1)$_2$]), 2092843 (for [Cu(L2)$_2$]), 2092839 (for [Zn(L1)$_2$]), 2092841 (for [Cu(L1)$_2$]SbF$_6$), 2092844 (for [Cu(L2)$_2$]SbF$_6$), and 2092842 (for [Cu(L1)$_2$](PF$_6$)$_2$) contain the supplementary crystallographic data for this paper. These data are provided free of charge by the joint Cambridge Crystallographic Data Centre and Fachinformationszentrum Karlsruhe Access Structures service.
[37] D. Emeljanenko, A. Peters, N. Wagner, J. Beck, E. Kaifer, H.-J. Himmel, *Eur. J. Inorg. Chem.* **2010**, 1839 – 1846.
[38] T. M. Ivanova, K. I. Maslakov, A. A. Sidorov, M. A. Kiskin, R. V. Linko, S. V. Savilov, V. V. Lunin, I. L. Eremenko, *J. Electron Spectrosc. Relat. Phenom.* **2020**, *238*, 146878-1-5.
[39] D. G. Brown, U. Weser, *Z. Naturforsch. B* **1979**, *34*, 989 – 994.
[40] A. D. Fedorenko, L. N. Mazalov, I. M. Oglezneva, E. Yu. Fursova, V. I. Ovcharenko, *J. Struct. Chem.* **2016**, *57*, 1121 – 1126.
[41] a) G. N. La Mar, *NMR of Paramagnetic Molecules: Principles and Applications*, Academic Press, New York, London, **1973**; b) I. Bertini, C. Luchinat, G. Parigi, E. Ravera, *NMR of Paramagnetic Molecules (Second Edition)*, Elsevier, Boston, **2017**; c) A. J. Pell, G. Pintacuda, C. P. Grey, *Prog. Nucl. Magn. Reson. Spectrosc.* **2019**, *111*, 1.
[42] a) H. Hilbig, P. Hudeczek, F. H. Köhler, X. Xie, P. Bergerat, O. Kahn, *Inorg. Chem.* **1998**, *37*, 4246 – 4257; b) D. L. Reger, A. E. Pascui, P. J. Pellechia, A. Ozarowski, *Inorg. Chem.* **2013**, *52*, 12741 – 12748; c) P. W. Kopf, R. W. Kreilick, *J. Am. Chem. Soc.* **1969**, *91*, 6569 – 6573; d) M. Damjanović, T. Morita, K. Katoh, M. Yamashita, M. Enders, *Chem. Eur. J.* **2015**, *21*, 14421 – 14432; e) T. E. Machonkin, W. M. Westler, J. L. Markley, *Inorg. Chem.* **2005**, *44*, 779 – 797; f) H. Liimatainen, T. O. Pennanen, J. Vaara, *Can. J. Chem.* **2009**, *87*, 954 – 964.
[43] P. Roquette, A. Maronna, M. Reinmuth, E. Kaifer, M. Enders, H.-J. Himmel, *Inorg. Chem.* **2011**, *50*, 1942 – 1955.
[44] A. Maronna, O. Hübner, M. Enders, E. Kaifer, H.-J. Himmel, *Chem. Eur. J.* **2013**, *19*, 8958 – 8977.

[45] B. Eberle, M. Damjanovic, M. Enders, S. Leingang, J. Pfisterer, C. Krämer, O. Hübner, E. Kaifer, H.-J. Himmel, *Inorg. Chem.* **2016**, *55*, 1683 – 1696.
[46] a) I. Bertini, C. Luchinat, G. Parigi, E. Ravera, *NMR of Paramagnetic Molecules (Second Edition)*, Elsevier, Amsterdam, **2017**, Chapter 11—*Magnetically coupled systems*, pp. 347 – 381; b) "The ^{1}H NMR parameters of magnetically coupled dimers-The Fe_2S_2 proteins as an example": L. Banci, I. Bertini, C. Luchinat, in *Bioinorganic Chemistry*, *Vol. 72*, Springer, Berlin, Heidelberg, **1990**, pp. 113 – 136.
[47] P. Chaudhuri, M. Hess, K. Hildenbrand, E. Bill, T. Weyhermüller, K. Wieghardt, *Inorg. Chem.* **1999**, *38*, 2781 – 2790.
[48] H. Oshio, T. Watanabe, A. Ohto, T. Ito, U. Nagashima, *Angew. Chem. Int. Ed. Engl.* **1994**, *33*, 670 – 671; *Angew. Chem.* **1994**, *106*, 691 – 692.
[49] D. J. R. Brook, V. Lynch, B. Conklin, M. A. Fox, *J. Am. Chem. Soc.* **1997**, *119*, 5155 – 5162.
[50] M. T. Green, T. A. McCormick, *Inorg. Chem.* **1999**, *38*, 3061 – 3065.
[51] H. Oshio, T. Ito, *Coord. Chem. Rev.* **2000**, *198*, 329 – 346.
[52] D. J. R. Brook, S. Fornell, B. Noll, G. T. Yee, T. H. Koch, *J. Chem. Soc. Dalton Trans.* **2000**, 2019 – 2022.
[53] D. J. R. Brook, G. T. Yee, M. Hundley, D. Rogow, J. Wong, K. Van-Tu, *Inorg. Chem.* **2010**, *49*, 8573 – 8577.
[54] a) Y. Wang, J. L. DuBois, B. Hedman, K. O. Hodgson, T. Stack, *Science* **1998**, *279*, 537 – 540; b) P. Chaudhuri, M. Hess, U. Flörke, K. Wieghardt, *Angew. Chem. Int. Ed.* **1998**, *37*, 2217 – 2220; *Angew. Chem.* **1998**, *110*, 2340 – 2343; c) F. Thomas, G. Gellon, I. Gautier-Luneau, E. Saint-Aman, J. L. Pierre, *Angew. Chem. Int. Ed.* **2002**, *41*, 3047 – 3050; *Angew. Chem.* **2002**, *114*, 3173 – 3176; d) T. K. Paine, T. Weyhermüller, K. Wieghardt, P. Chaudhuri, *Dalton Trans.* **2004**, 2092 – 2101; e) C. Mukherjee, U. Pieper, E. Bothe, V. Bachler, E. Bill, T. Weyhermüller, P. Chaudhuri, *Inorg. Chem.* **2008**, *47*, 8943 – 8956; f) O. Das, T. K. Paine, *Dalton Trans.* **2012**, *41*, 11476 – 11481.

Manuscript received: July 14, 2021
Revised manuscript received: July 30, 2021
Accepted manuscript online: August 23, 2021
Version of record online: September 17, 2021

